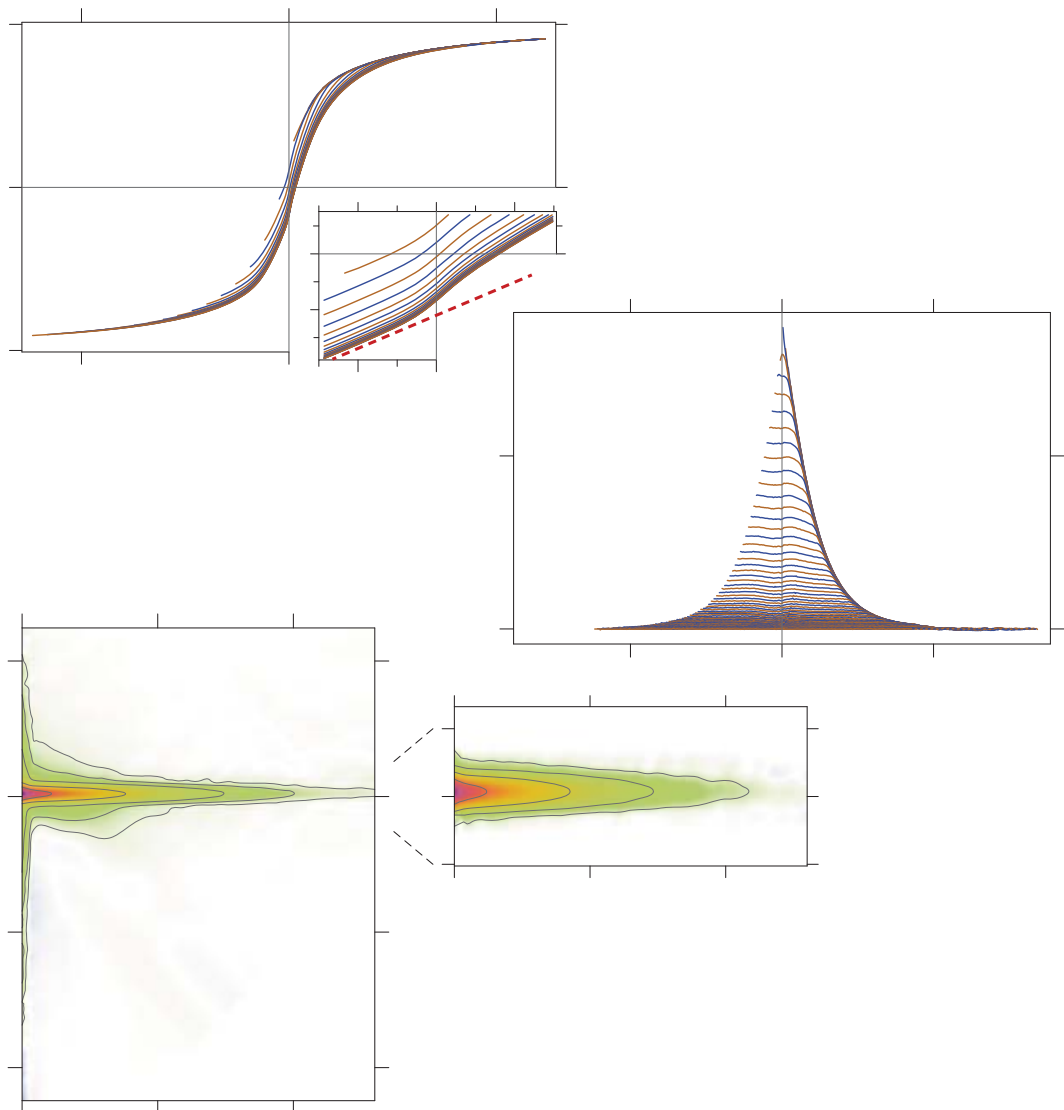


VARIFORC processing examples

Single-domain viscosity



About this example

The measured material consists of nearly equidimensional, single-domain magnetite crystals (extracted magnetosomes) dispersed in clay. This example handles the intrinsic FORC processing problems encountered with samples containing magnetic particles with arbitrarily small switching fields, as for instance viscous single-domain grains. In this case, the hysteresis loop, as well as FORC measurements, are quasi-discontinuous near $H=0$, regardless of field step size.

Processing difficulties arise from the fact that FORC diagram calculations require the measured curves and their first derivative to be locally smooth, in order to be fitted by second-order polynomials over a minimum number of points given by the chosen smoothing factor. Magnetization curves generated by arbitrarily small switching fields are not locally smooth, because a magnetization jump and a discrete slope change will always occur over few points around $H=0$, regardless of how small the measurement field steps are chosen. VARIFORC can handle such measurements very effectively by redefining the measurement curves in a manner that eliminates discontinuities and by limiting the smoothing factor over critical fields such as $H=0$.

FORC measurements

- Measuring instrument: PMC MicroMag 2900 AGM.
 - Specimen preparation: Powder fixed with cyanoacrylate glue.
 - FORC measurement protocol:
 - Hc1 = 0 , Hc2 = 0.05 T
 - Hb1 = -0.01 T, Hb2 = +0.03 T
 - Hsat = 0.2 T
 - Averaging time = 0.1 s
 - Pause at calibration = 0.5 s
 - Pause at reversals = 0.5 s
 - Pause at saturation = 0.2 s
 - Smoothing = 5 (adds a 5-point margin to the measured range)
 - Derived measurement parameters:
 - Number of curves: 650
 - Calibration measurements at 0.085 T
 - Mean size of field steps = 0.33 mT (maximum resolution of the FORC diagram)
 - **Notes on measurements.** AGM measurements tend to be affected by irregular drift. Therefore, it is essential to minimize the total measurement time at a minimum by choosing a short averaging time (in this example: 0.1 s). Increased measurement noise associated with short averaging times is compensated by repeated measurements (e.g. 2 sets of FORC measurements at 0.1 s averaging time instead of one set at 0.2 s averaging time). Multiple FORC measurements are automatically averaged during VARIFORC processing. In this example, the same specimen has been measured 5 times using the same FORC protocol.
-

About VARIFORC processing options used in this example

VARIFORC modules are controlled by processing options stored in so-called parameter files. Parameter files used to process FORC data related to this example can be found in the folder containing this document. These are:

1. Import and correct FORC measurements (ImportFORC module):

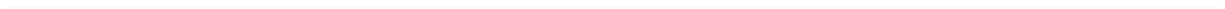
- D900_VARIFORC_ImportFORC_parameters.txt: no first-point correction
- D900-fpc_VARIFORC_ImportFORC_parameters.txt: first-point correction

2. Calculate the FORC diagram (CalculateFORC module):

- D900-SF5_VARIFORC_CalculateFORC_parameters.txt: conventional processing with a constant smoothing factor (SF = 5). For demonstration purposes only.
- D900-dforc-SF5_VARIFORC_CalculateFORC_parameters.txt: conventional processing of FORC differences with a constant smoothing factor (SF = 5). For demonstration purposes only.
- D900-dforc-opt_VARIFORC_CalculateFORC_parameters.txt: optimal variable smoothing processing of FORC differences.

3. Isolate the central ridge (IsolateCR module):

- D900_VARIFORC_IsolateCR_parameters.txt.
-



Measurements import, correction, and averaging

Five sets of identical measurements have been imported and averaged with **ImportFORC** in a single run (see parameter file `D900_VARIFORC_ImportFORC_parameters.txt`). Each set has been corrected individually for drift and outliers. Corrected measurements were subsequently averaged by weighting each set according to the estimated level of measurement noise, so that worse sets count less than better ones. This procedure minimizes measurement error contributions to the average and is part of the standard processing algorithm of **ImportFORC**. In this example, weights ranged from 0.43 (worse set) to 1.9 (best set).

The first point of each curve is anomalous (**Plates 1a,b**), because it is located above the trend set by the other points. This is a common problem of FORC measurements caused by the impossibility to reverse the electromagnet's field sweep without inducing a spurious signal in the measurement system. In this example, first-point artifacts are very small and become visible only after the lower branch of the hysteresis loop reconstructed from FORC measurements has been subtracted from each curve (**Plate 1b**). **ImportFORC** supports the elimination of first-point artifacts by replacing first-point measurements with a second-order polynomial extrapolation of adjacent measurements (see the VARIFORC example on first-point correction). This correction has been performed using the parameter file `D900-fpc_VARIFORC_ImportFORC_parameters.txt` and results are shown in **Plates 1c,d**. Successful removal of first-point artifacts is evident from the comparison of **Plates 1b,d**.

The hysteresis loop has a constricted, or “wasp-waisted” shape, which is characteristic for mixtures of superparamagnetic and stable single-domain particles [*Tauxe et al.*, 1996]. Moreover, the measured magnetization, as well as the slope of all curves, increase sharply between ± 1 mT (inset of **Plate 1c**). In this example, measurement field steps (~ 0.33 mT) cover the sharp magnetization changes occurring near $H = 0$ with ~ 6 points. These changes are poorly fitted by second-order polynomials, causing FORC processing problems even with smoothing factors as small as 2. Because this phenomenon is caused by magnetic viscosity, it will always extend over the same number of points near $H = 0$, regardless of field step size.

FORC measurements with subtracted hysteresis branch (**Plates 1b,d**) are free from the above-mentioned features near $H = 0$, which means that such features are common to all curves – including the two branches of the hysteresis loop – and do not contribute to the FORC diagram. As shown later, calculation of the FORC diagram from measurements with subtracted hysteresis branch eliminates processing problems near $H = 0$. This is possible because any curve added or subtracted to all FORC data, including one that reproduces the features seen near $H = 0$, does not affect the mixed derivative from which the FORC function is calculated.

The nearly horizontal curves in **Plates 1b,d** are a typical feature of non-interacting single-domain particles with squared hysteresis loops. All curves merge on the right with their exponential-like envelope through a sudden change in slope, which generates a so-called central ridge in the FORC diagram [*Egli et al.*, 2010]. The curve envelope coincides with the even component of the hysteresis loop, i.e. the difference between upper and lower branches [*Fabian and Dobeneck*, 1997].

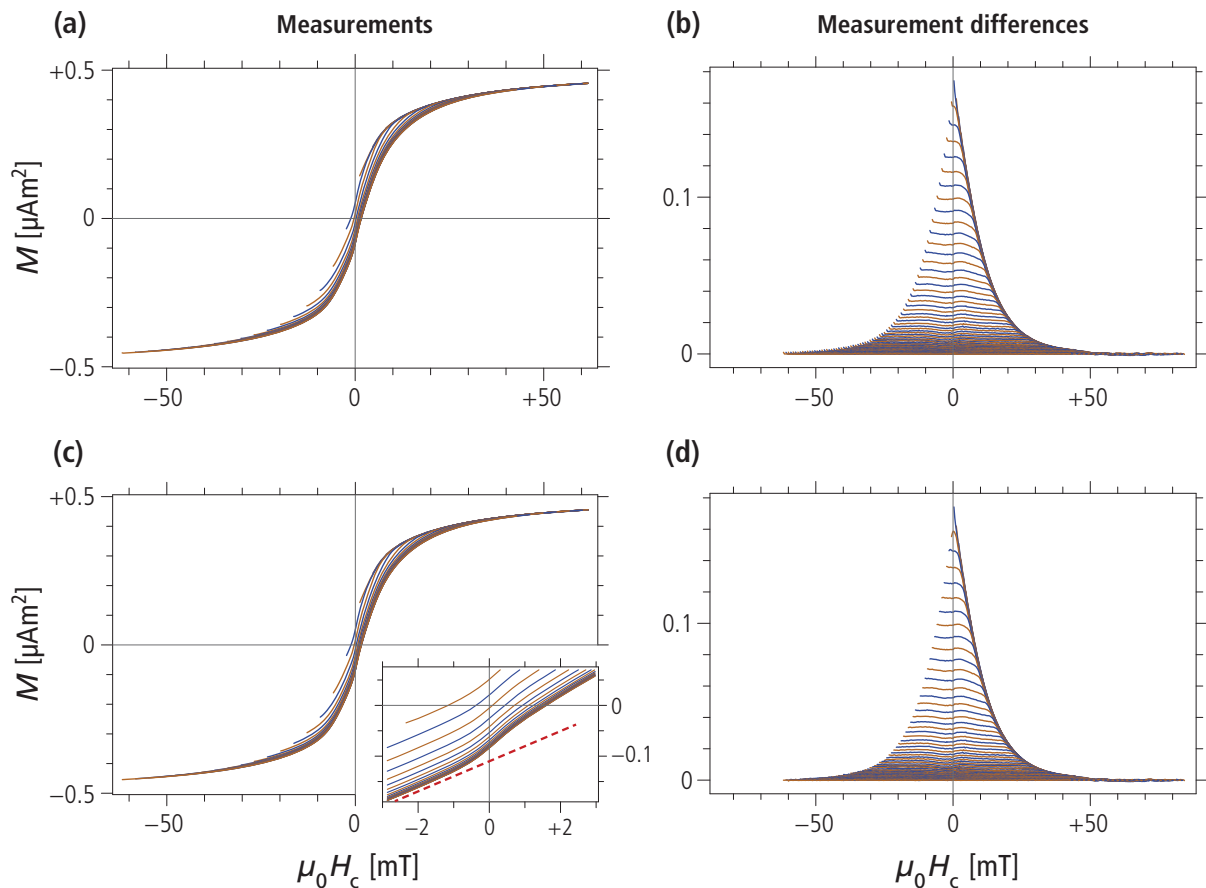


Plate I. Averaged FORC measurements. (a-b) Drift- and outlier-corrected measurements. (c-d) Same as (a-b) after first-point correction. Plots were generated by `ImportFORC` with minor editing. Left plots show the measured curves, (every 12th curve for clarity, see `INPUT 14` of the parameter file). Right plots show the same measurements after subtraction of the lower hysteresis branch reconstructed from the FORC measurements (see `INPUT 21` of the parameter file). Every 3rd curve is shown for clarity. The insert in (c) shows a detail of the measurements near $H=0$, where the magnetization slope of all curves changes abruptly -1 and $+1$ mT (see red dashed line for reference).

Hysteresis properties of the constricted, or “wasp-waisted” loop ($M_{rs}/M_s = 0.174$ and $H_{cr}/H_c = 4.73$) suggest a mixture of pseudo-single-domain (PSD) and superparamagnetic (SP) particles (Plate 2), although the sample is known to contain only single-domain magnetite crystals (magnetosomes). The inconsistency might be due to the sensitivity of mixing models on parameters, such as SP grain size and anisotropy, which are not known a-priori. On the other hand, single-domain particles could be clustered or still retain some structures of the original magnetosome chains [e.g. *Shcherbakov et al.*, 1997; *Kobayashi et al.*, 2006], in which case magnetostatic interaction would influence the hysteresis properties. However, the FORC diagram contains only minor magnetostatic interaction signatures, as shown in the next sections.

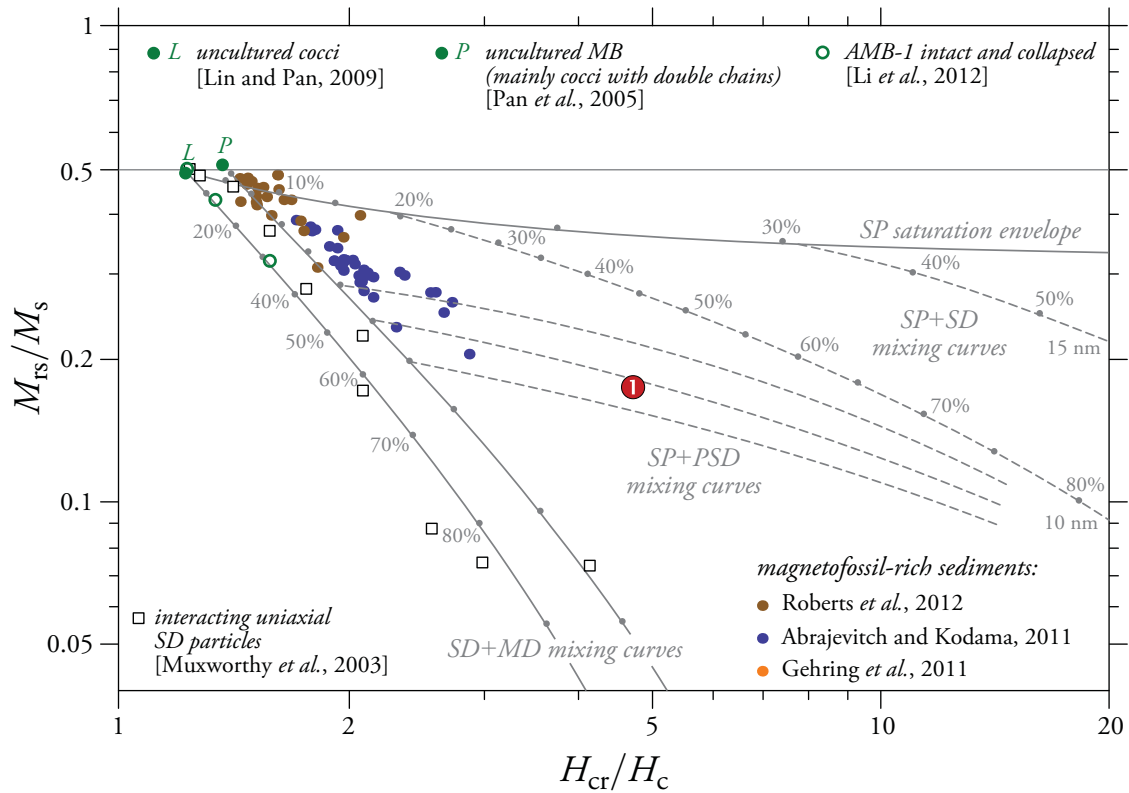


Plate 2. Hysteresis properties in the Day diagram. Day diagram after Dunlop [2002] showing the hysteresis properties of the dispersed magnetosomes (①).

FORC processing after lower hysteresis branch subtraction

This example shows some critical aspects of FORC processing encountered with viscous samples (Plate 3). The first problem arises from measurement artifacts affecting the first point of each curve (see corresponding VARIFORC example for an in-depth discussion). These artifacts create a vertical ridge along $H_c = 0$ (Plate 3a), which extends well beyond negative field amplitudes required for saturation. This ridge is a measurement artifact that should not be confused with the signature of magnetic viscosity [Pike *et al.*, 2001]. This signature emerges only when processing first-point corrected FORC measurements (Plate 3b). In this case, the vertical ridge amplitude peaks at $H_b = 0$ and vanishes within $H_b = \pm 20$ mT, i.e. over a range of fields where the sample is not saturated. Correction of first-point artifacts is performed when importing FORC measurements with **Import FORC** (see the parameter file `D900-fpc_VARIFORC_Import FORC_parameters.txt`).

The next FORC processing problem is related to sharp magnetization changes occurring in a narrow range of fields around $H = 0$ (see previous section). Second-order polynomial regression used to calculate the FORC diagram is not well-suited for reproducing such changes, so that processing artifacts appear along the $H_b = -H_c$ diagonal where $H = 0$ (Plates 3a,b). Strongly negative anomalies at the two extremities of the diagonal are particularly problematic, and worsen if the smoothing factor is increased. In fact, these artifacts cannot be properly eliminated by conventional processing of the measured curves.

As discussed in the previous section, sharp magnetization changes near $H = 0$ are completely removed if the lower branch of the hysteresis loop is subtracted from each curve. Modified FORC data with subtracted hysteresis are automatically exported by **ImportFORC** and can be used instead of direct measurements (INPUT 01 in the parameter file `D900-dforc_VARIFORC_CalculateFORC_parameters.txt`). The beneficial effect of using the modified FORC dataset is clearly visible in Plates 3c, where strong negative artifacts at the two extremities of the $H_b = -H_c$ diagonal are completely removed, and overall fluctuations along this diagonal are strongly reduced as well. Subtraction of the same magnetization curve – such as the lower branch of the hysteresis loop – from all measurements does not affect the resulting FORC diagram beyond the elimination of regression artifacts, since the subtracted curve does not contribute to the mixed derivative upon which the FORC function is defined. In general, regression artifacts caused by features that are common to all measured curves can always be eliminated if FORC diagrams are calculated with the modified FORC data instead of the original measurements. Because subtraction of the lower hysteresis branch reconstructed from FORC measurements introduces some additional measurement noise, modified FORC data should be used only if problems are encountered when processing original measurements.

Once all regression artifacts have been avoided, a variable smoothing procedure can be applied in order to remove measurement noise and improve the FORC diagram quality (Plates 3d), like in the other VARIFORC examples.

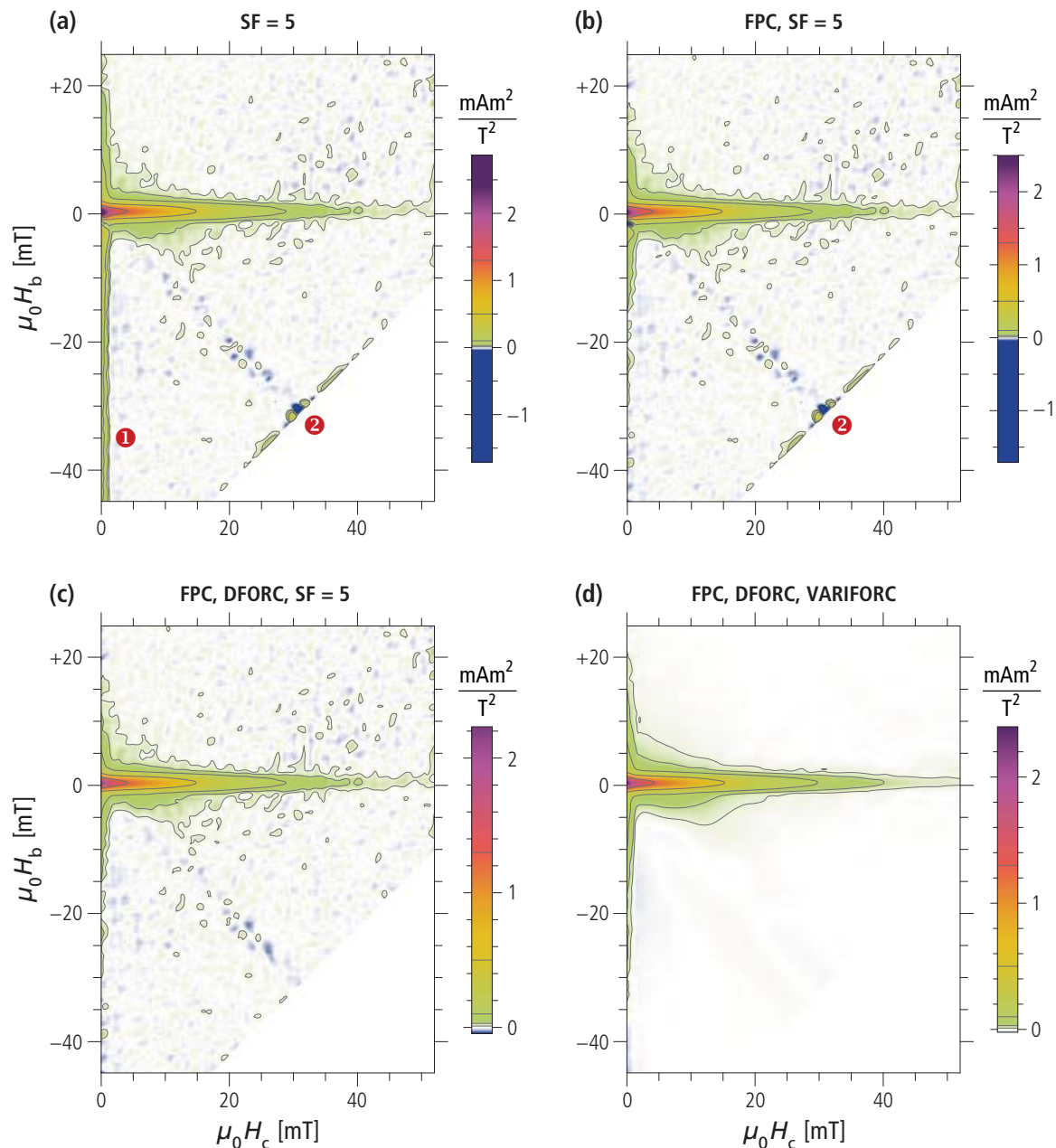


Plate 3. FORC processing optimization for viscous single-domain particles. (a) FORC diagram calculated from the original dataset without first-point correction and using a constant smoothing factor $SF = 5$ (see `D900_VARIFORC_ImportFORC_parameters.txt` and `D900_SF5_VARIFORC_CalculateFORC_parameters.txt`). Processing artifacts related to anomalous first-point measurements (❶), and sharp magnetization changes near $H = 0$ (❷), are evident. (b) Same as (a), after correcting anomalous first-point measurements with `ImportFORC` (`D900-fpc_VARIFORC_ImportFORC_parameters.txt`). The true signature of magnetic viscosity along $H_c = 0$ is now visible. (c) Same as (b), when using a modified set of FORC measurements obtained by subtraction of the lower hysteresis from all curves (see `D900-fpc_VARIFORC_ImportFORC_parameters.txt` and `D900-dforc_SF5_VARIFORC_CalculateFORC_parameters.txt`). Artifacts along the $H_c = -H_c$ are almost completely removed (notice the negative end of the color scale in comparison to (a)). (d) Same as (c), using variable smoothing (`D900-dforc_VARIFORC_CalculateFORC_parameters.txt`).

Complete VARIFORC analysis

The peculiar FORC properties of dispersed equidimensional magnetosomes are summarized in Plate 4. Although similar properties are rarely found in nature, this example represents a possible end-member for a wide range of magnetic properties associable with secondary magnetic minerals formed in sediments [e.g., *Abrajevitch and Kodama, 2011*; *Roberts et al., 2012*; *Yamazaki et al., 2013*; *Chang et al., 2014*], sedimentary rocks [e.g., *Abrajevitch et al., 2011*], and soils [*Geiss et al., 2008*].

The FORC diagram (Plate 4a) is characterized by a single maximum at the intersection point ($H_c = 0$, $H_b \approx 0$) between a vertical ridge and the central ridge. The two ridges represent the main features of the diagram, with little additional contributions distributed over the remaining FORC space. This is the typical signature of samples containing non-interacting viscous single-domain particles [*Pike et al., 2001*]. The vertical ridge is produced by viscous single-domain particles with magnetization decay times comparable with the time required to measure the first few points of each curve. Residual FORC contributions after subtraction of the central ridge (Plate 4b) are characterized by one order of magnitude smaller amplitudes and are limited to $H_c \leq 20$ mT. These contributions might arise from magnetostatic interactions or magnetic particles with cubic magnetocrystalline anisotropy.

The central ridge (Plate 4c) peaks at $H_c = 0$, unlike central ridges isolated from magnetofossil-rich sediments (see corresponding VARIFORC example). Coercivity distributions derived from FORC measurements and from the central ridge (Plate 4d) are nearly identical, which means that the FORC diagram is produced by non-interacting magnetic particles with rectangular hysteresis loops. This sample is therefore a physical realization of the Preisach-Néel hysteresis model [*Preisach, 1935*; *Néel, 1958*], where irreversible magnetic processes are represented by rectangular hysterons associated with individual single-domain particles. Such particles lack the reversible magnetic moment rotation expected for single-domain particles [*Stoner and Wohlfarth, 1948*], as demonstrated by the absence of negative amplitudes over the lower quadrant of the FORC diagram [*Newell, 2005*]. This phenomenon can be explained by thermally activated moment switching in fields that are much smaller than expected without thermal activations [*Ludwig et al., 2013*].

The exponential shape of coercivity distributions indicates that most particles can be switched in vanishingly small fields. This is, at least in part, the consequence of thermal activations in viscous SD particles: similar properties are seen in volcanic tuff samples containing elongated magnetite particles with a very large intrinsic anisotropy [*Pike et al., 2001*; *Jackson et al., 2006*]. In this example, small switching fields are also favored by the relatively small intrinsic anisotropy of equidimensional of magnetosomes.

In summary, all magnetic properties of this sample can be explained by a collection of non-interacting, viscous single domain particles with small intrinsic anisotropy.

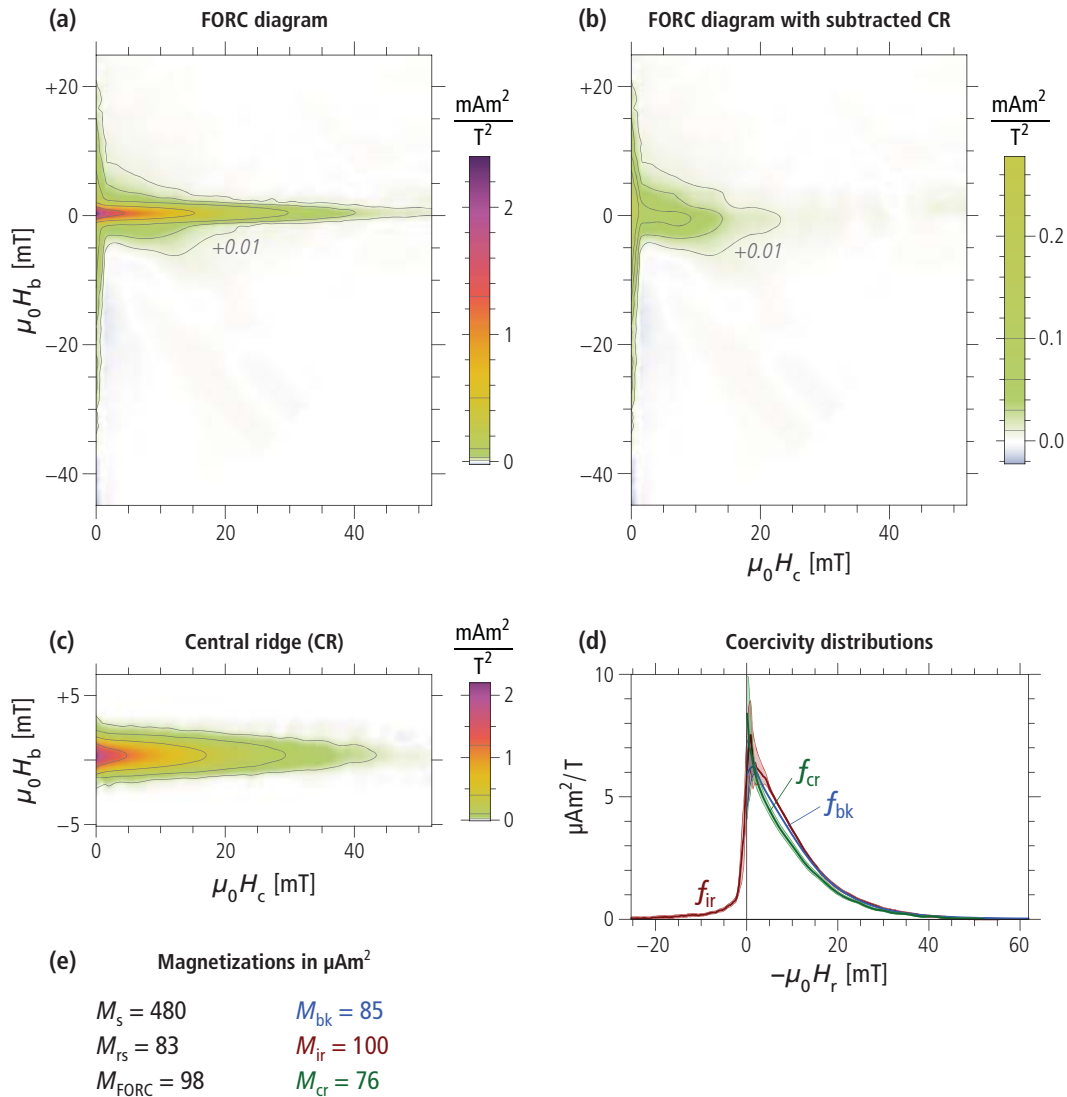
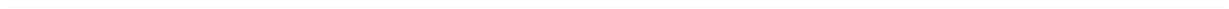


Plate 4. Complete VARIFORC analysis of dispersed magnetosomes. (a) FORC diagram obtained with `CalculateFORC` (contour lines have been added with `PlotFORC`). Notice that the smallest contour level corresponds to 0.4% of the maximum FORC amplitude and is still fully significant. (b) FORC diagram remaining after subtraction of the central ridge with `IsolateCR`. The isolated central ridge is shown in (c) with a 2× vertical exaggeration, which highlights a small upward shift of the whole ridge. The shift is due to thermal activation effects. All FORC diagrams share the same color scale. (d) Three types of coercivity distribution derived from FORC measurements, with shaded bands around each curve representing 2σ confidence levels. The first two distributions, f_{bk} and f_{ir} derive from remanent magnetizations and the irreversible component of hysteresis, respectively. They are generated by `CalculateFORC` as part of the standard output. The third distribution, f_{cr} , is associated with the central ridge and is generated by `IsolateCR`. All three distributions are plotted by `IsolateCR` as seen in this example. f_{ir} is the only distribution that exists for positive and negative fields, like the hysteresis loop from which it is derived. Negative arguments of f_{ir} represent irreversible magnetization processes that occur without reversing the field direction. Only non-interacting, uniaxial single-domain particles produce a strictly positive f_{ir} . (e) Total magnetizations derived from FORC measurements (M_s and M_{rs}), integration of the FORC diagram (M_{FORC}), and integration of the coercivity distributions shown in (d) (M_{bk} , M_{ir} , and M_{cr}).



Literature

- Abrajevitch, A., K. Kodama (2011). Diagenetic sensitivity of paleoenvironmental proxies: A rock magnetic study of Australian continental margin sediments, *Geochemistry, Geophysics, Geosystems* 12, Q05Z24, doi:10.1029/2010GC003481.
- Abrajevitch, A., R.S. Hori, K. Kodama (2011). Magnetization carriers and remagnetization of bedded chert, *Earth and Planetary Science Letters* 305, 135-142, doi:10.1016/j.epsl.2011.02.047.
- Chang, L., A.P. Roberts, M. Winklhofer, D. Heslop, M.J. Dekkers, W. Krijgsman, J.D. Fitz Gerald, P. Smith (2014). Magnetic detection and characterization of biogenic magnetic minerals: A comparison of ferromagnetic resonance and first-order reversal curve diagrams, *Journal of Geophysical Research: Solid Earth* 119, 6136-6158, doi:10.1002/2014JB011213.
- Dunlop, D.J. (2002). Theory and application of the Day plot (M_{rs}/M_s versus H_{cr}/H_c) 2. Application to data for rocks, sediments, and soils, *Journal of Geophysical Research* 107, 2057, doi:10.1029/2001JB000487.
- Egli, R., A.P. Chen, M. Winklhofer, K.P. Kodama, C.S. Horng (2010). Detection of noninteracting single domain particles using first-order reversal curve diagrams, *Geochemistry, Geophysics, Geosystems* 11, Q01Z11, doi:10.1029/2009GC002916.
- Fabian, K., T. von Dobeneck (1997). Isothermal magnetization of samples with stable Preisach function: A survey of hysteresis, remanence, and rock magnetic parameters, *Journal of Geophysical Research* 102, 17659-17677.
- Gehring, A.U., J. Kind, M. Charilaou, I. García-Rubio (2011). The detection of magnetotactic bacteria and magnetofossils by means of magnetic anisotropy, *Earth and Planetary Science Letters* 309, 113-117.
- Geiss, C.E., R. Egli, and C.W. Zanner (2008). Direct estimates of pedogenic magnetite as a tool to reconstruct past climates from buried soils, *Journal of Geophysical Research* 113, B11102, doi:10.1029/2008JB005669.
- Jackson, M., B. Carter-Sitgitz, R. Egli, P. Solheid (2006). Characterizing the superparamagnetic grain distribution $f(V, H_k)$ by thermal fluctuation tomography, *Journal of Geophysical Research* 111, B12S07, doi:10.1029/2006JB004514.
- Kobayashi, A., J.L. Kirschvink, G.Z. Nash, R.E. Kopp, D.A. Sauer, L. Elizabeth Bertani, W.F. Voorhout, T. Taguchi (2006). Experimental observation of magnetosome chain collapse in magnetotactic bacteria: Sedimentological, paleomagnetic, and evolutionary implications, *Earth and Planetary Science Letters* 245, 538-550.
- Li, J., W. Wu, Q. Liu, and Y. Pan (2012). Magnetic anisotropy, magnetostatic interactions, and identification of magnetofossils, *Geochemistry, Geophysics, Geosystems* 13, Q10Z51, doi:10.1029/2012GC004384.
- Lin, W., Y. Pan (2009). Uncultivated magnetotactic cocci from Yuandadu Park in Beijing, China, *Applied and Environmental Microbiology* 75, 4046-4052.
- Ludwig, P., R. Egli, S. Bishop, V. Chernenko, T. Frederichs, G. Rugel, S. Merchel, M.J. Orgeira (2013). Characterization of primary and secondary magnetite in marine sediment by combining chemical and magnetic unmixing techniques, *Global and Planetary Change* 110, 321-339, doi:10.1016/j.gloplacha.2013.08.018.
- Muxworthy, A., W. Williams, D. Virdee (2003). Effect of magnetostatic interactions on the hysteresis parameters of single-domain and pseudo-single-domain grains, *Journal of Geophysical Research* 108, doi:10.1029/2003JB002588.
- Néel, L. (1958). Sur les effets d'un couplage entre grains ferromagnétiques, *Comptes Rendus de l'Académie des Sciences*, 246, 2313-2319.
-

- Newell, A.J. (2005). A high-precision model of first-order reversal curve (FORC) functions for single-domain ferromagnets with uniaxial anisotropy, *Geochemistry, Geophysics, Geosystems* 6, Q05010, doi:10.1029/2004GC000877.
- Pan, Y., N. Petersen, M. Winklhofer, A.F. Davila, Q. Liu, T. Frederichs, M. Hanzlik, R. Zhu (2005). Rock magnetic properties of uncultured magnetotactic bacteria, *Earth and Planetary Sciences* 237, 311-325.
- Pike, C.R., A.P. Roberts, K.L. Verosub (2001). First-order reversal curve diagrams and thermal relaxation effects in magnetic particles, *Geophysical Journal International* 145, 721-730.
- Preisach, F. (1935). Über die magnetische Nachwirkung, *Zeitschrift für Physik*, 94, 277-302.
- Roberts, A.P., L. Chang, D. Heslop, F. Florindo, J.C. Larrasoana (2012). Searching for single domain magnetite in the “pseudo-single-domain” sedimentary haystack: Implications of biogenic magnetite preservation for sediment magnetism and relative paleointensity determination, *Journal of Geophysical Research* 117, B08104, doi:10.1029/2012JB009412.
- Shcherbakov, V.P., M. Winklhofer, M. Hanzlik, N. Petersen (1997). Elastic stability of chains of magnetosomes in magnetotactic bacteria, *European Biophysical Journal* 26, 319-326.
- Stoner, E.C., and E.P. Wohlfarth (1948). A mechanism of magnetic hysteresis in heterogeneous alloys, *Philosophical Transactions of the Royal Society of London*, A240, 599-642.
- Tauxe, L., T.A.T. Mullender, and T. Pick (1996). Potbellies, wasp-waists, and superparamagnetism in magnetic hysteresis, *Journal of Geophysical Research* 101, 571-583.
- Yamazaki, T., Y. Yamamoto, G. Acton, E.P. Guirby, C. Richter (2013). Rock-magnetic artifacts on long-term relative paleointensity variations in sediments, *Geochemistry, Geophysics, Geosystems* 14, doi:10.1029/2012GC004546.
-